Cell Reports, Volume *22*

Supplemental Information

Hippocampal Global Remapping Can Occur without Input from the Medial Entorhinal Cortex

Magdalene I. Schlesiger, Brittney L. Boublil, Jena B. Hales, Jill K. Leutgeb, and Stefan Leutgeb

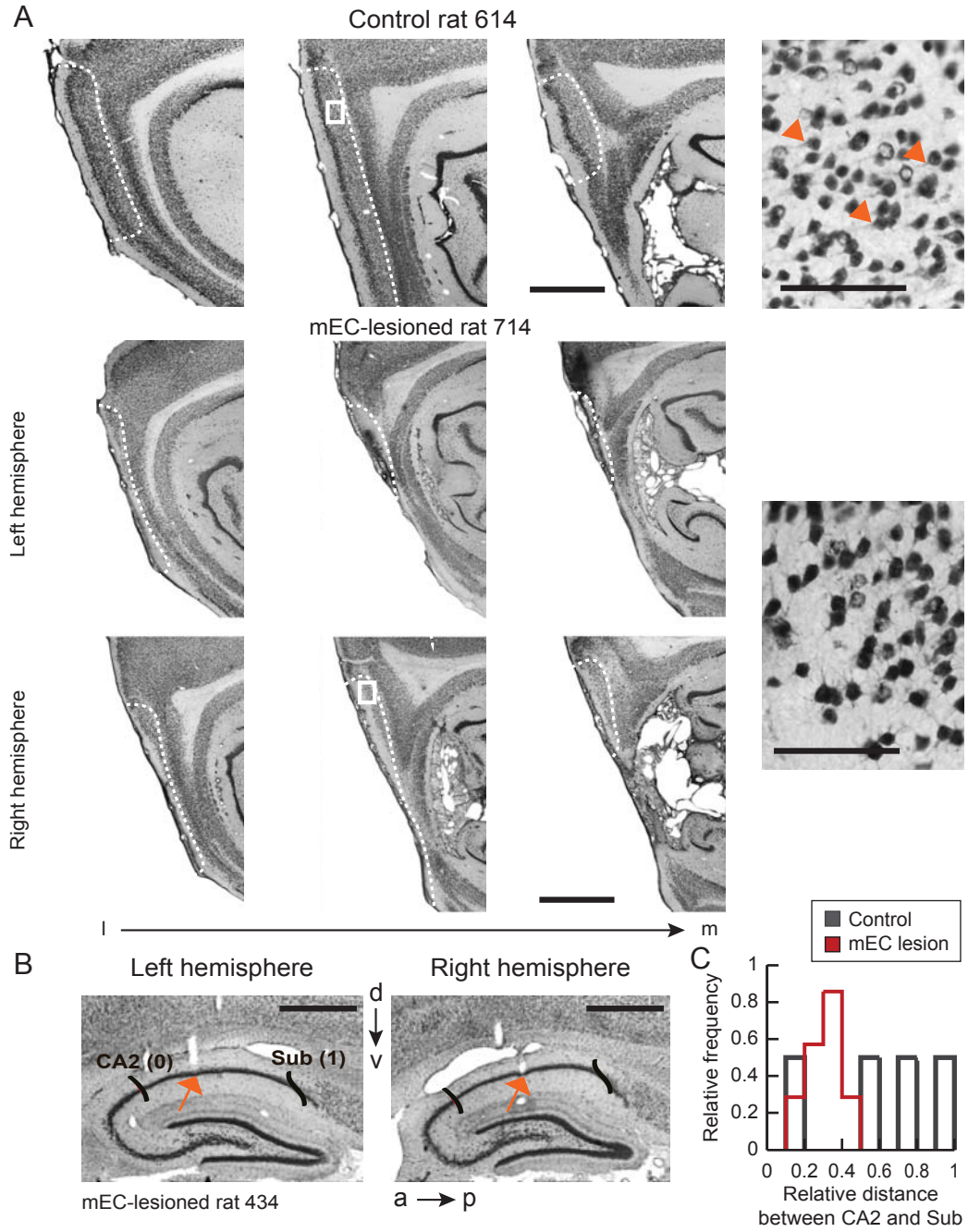

Figure S1. Example histological images of control and mEC-lesioned rats. Related to Figures 2–5. (**A**) Sagittal sections at three different lateral to medial levels are shown for one hemisphere in a control rat and for both hemispheres in mEC-lesioned rat 714. Superficial layers II and III are outlined by white stippled lines. The rightmost panel for each rat is a high-magnification image of layer III cells from the area indicated by a white box. Arrows in control image point to apical dendrites that are oriented towards the cortical surface. In the mEC-lesioned rat, cells in the superficial layers were either completely absent or, when small patches of cells were discernable, showed signs of disorganization and necrosis such as multipolar processes and fragmented nuclei. Scale bars are 1 mm and 125 µm. See Hales et al., 2014 and Schlesiger et al., 2015 for images from additional mEC-lesioned rats. (**B**) Tetrode tracks in the two hemispheres of mEC-lesioned rat 434 are shown in the sagittal plane. Arrows point to the end of tetrode tracks within the CA1 cell layer. (**C**) Distribution of relative tetrode locations along the proximal-to-distal axis. For each tetrode, the position between CA2 (0) and the subiculum (Sub, 1) was determined. In mEC-lesioned rats, all tetrodes were located in proximal to intermediate CA1.

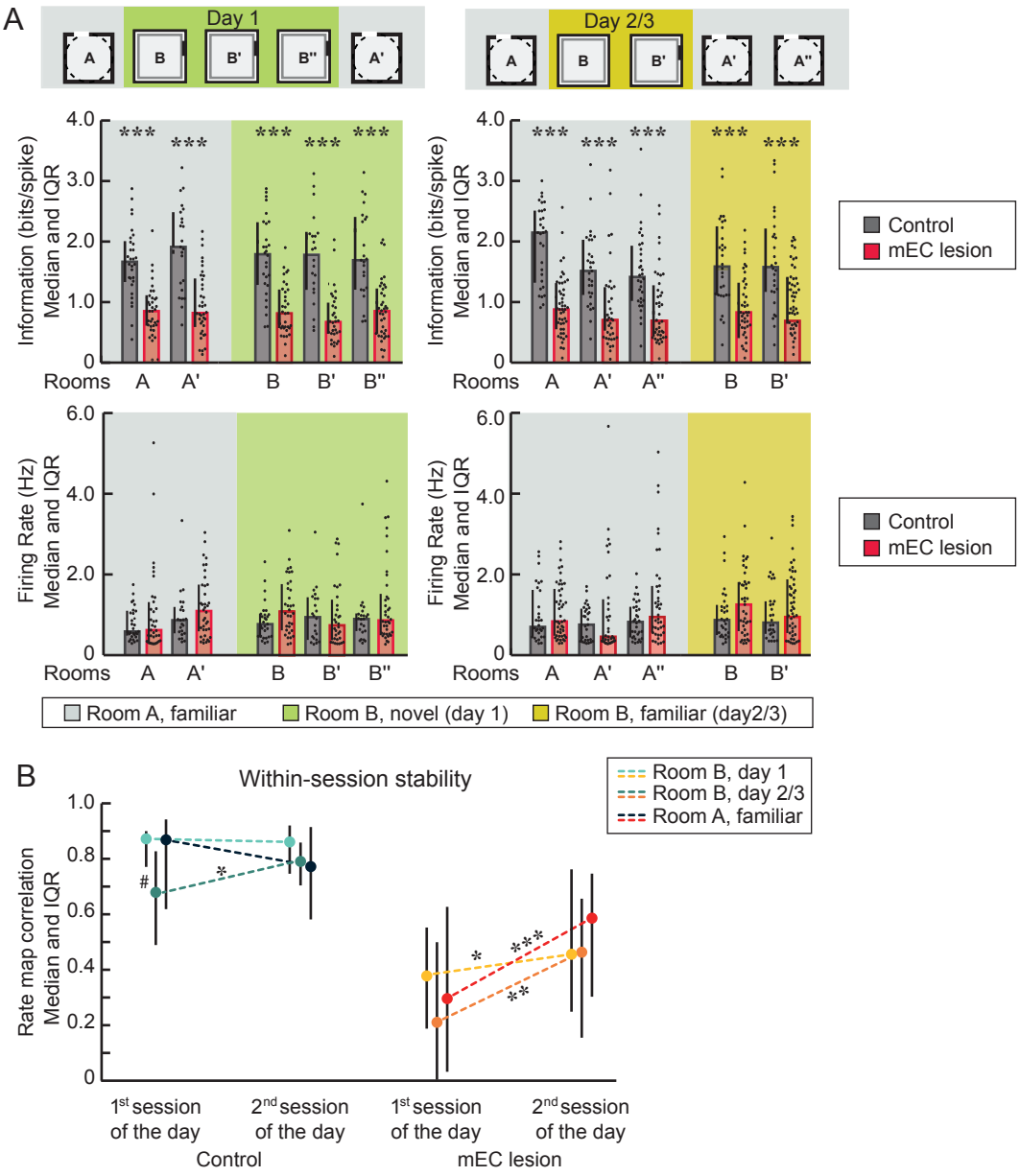

Figure S2. Information scores, mean firing rates and map stability in individual recording sessions. Related to Figure 2A. (**A**) Irrespective of the familiarity of the environment, information scores were reduced (all p values < 0.001, Mann-Whitney U tests), but firing rates were similar in mEC-lesioned compared to control rats (all p values ≥ 0.43, Mann-Whitney U tests). Black dots are values for individual cells, bars are medians, and error bars are IQR. *** $p \leq 0.001$, mEC lesioned vs control. (**B**) For three environments with different degrees of experience, the first and second 10-min session of the day was split into two 5-min intervals, and the within-session map stability was calculated. Of note, the within-session map stability in moderately and highly familiar environments in mEC-lesioned rats was as low as in entirely novel environments (p = 0.24, Kruskal-Wallis test). In controls, within-session map stability was lower in the first session of day 3 than in the other conditions (p = 0.00016, Kruskal-Wallis test). Within-session map stability increased from the first to the second session of the day in mEC-lesioned rats irrespective of the novelty of the environment (all p values ≤ 0.034, Wilcoxon signed-rank tests). Because stability was already high in the first session in control rats, there was no clear trend for a further increase (day 1 and highly familiar, both p values ≥ 0.099; day 3, p = 0.0099, Wilcoxon signed-rank tests). Symbols and error bars are the median and IQR. Holm-Bonferroni correction was applied for multiple comparisons. First vs. second session of the day, * $p \leq 0.05$, ** $p \leq 0.005$, *** $p \leq 0.001$; comparison between levels of familiarity, # $p \leq 0.001$.

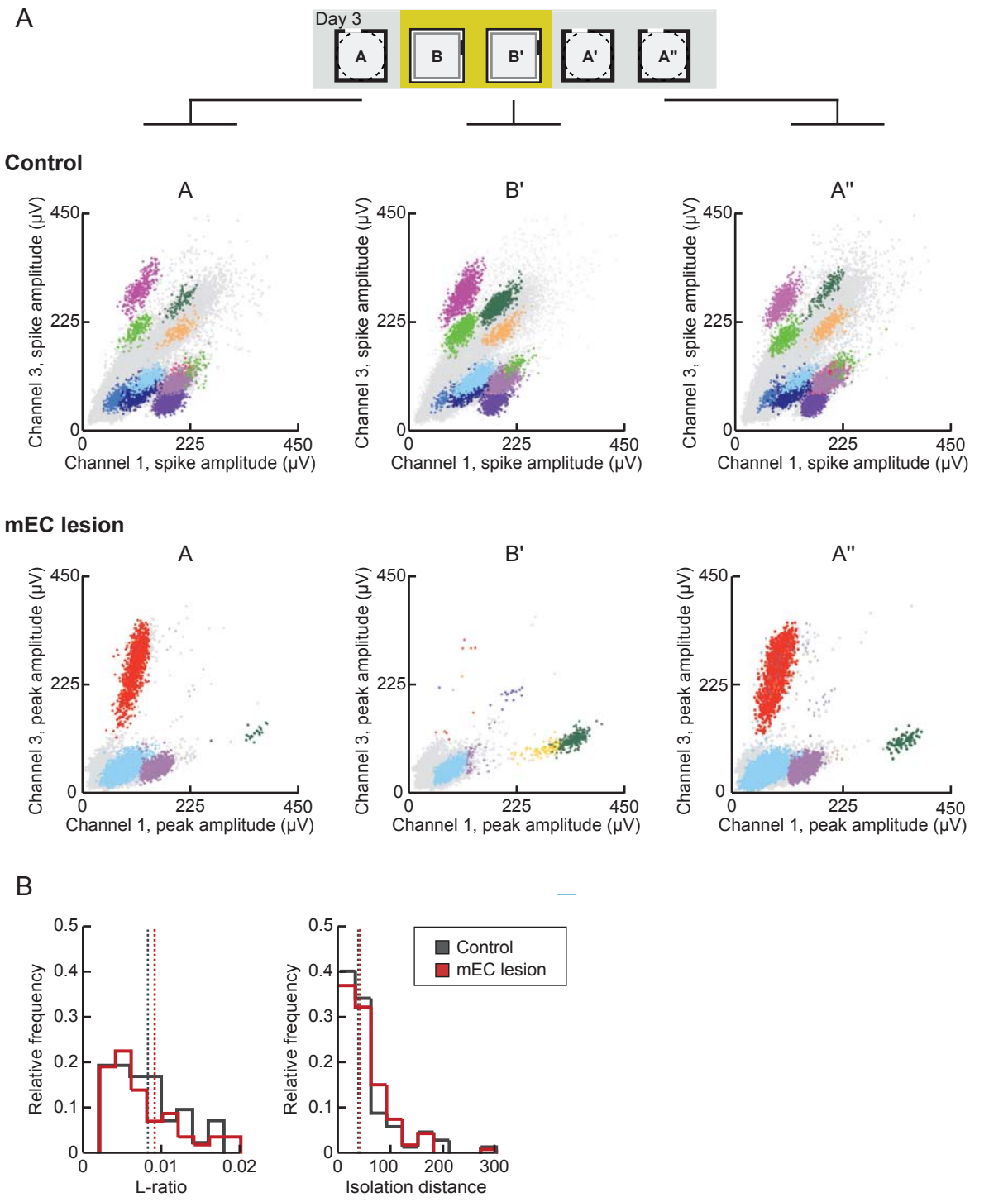

Figure S3. Cluster quality did not differ between control and mEC-lesioned rats. Related to Figure 2. (**A**) For each recording day, single-units were tracked across sessions. Scatter plots for spike amplitudes recorded on two of the four channels of a representative tetrode in a control (middle panel) and an mEC-lesioned rat (bottom panel) are shown for sessions A, B' and A'' of day three of the recording experiment. (**B**) Cluster quality measures did not differ between control and mEC-lesioned rats (L-ratio and Isolation distance, *p* values ≥ 0.43, Mann-Whitney U tests).

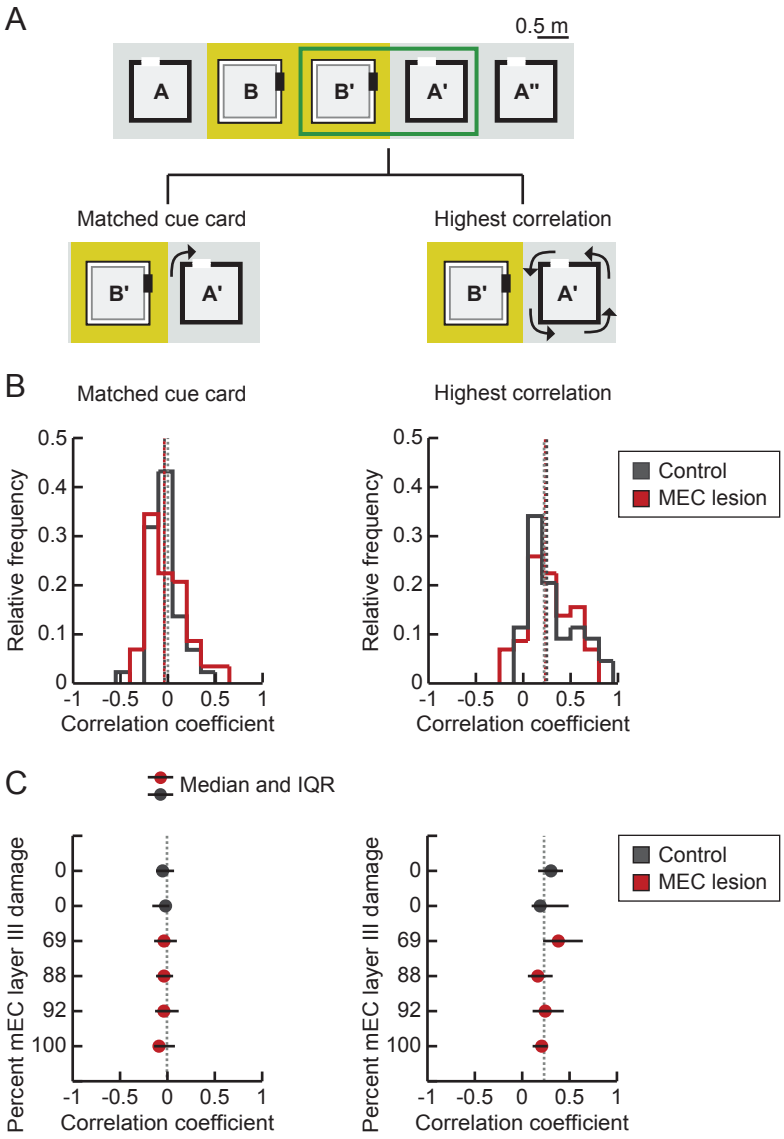

Figure S4. Low map similarity across rooms was not the result of the rotation of a stereotyped map. Related to Figure 4. (**A**) Schematic of the analysis performed to examine whether the low map similarity across rooms was the result of the coordinated shift of a constant map. For each cell, a pair of maps (top, green outline) was compared, after the map obtained in A' was rotated in one of two different ways. (1) It was rotated to match the orientation of the cue card across rooms (bottom left, 'Matched cue card'), or (2) it was rotated in steps of 90 degrees and the comparison with the highest correlation coefficient was selected for each cell (bottom right, 'Highest correlation'). To obtain the chance level, each analysis was repeated after shuffling of the cell identity. (**B**) In both the 'Matched cue card' and the 'Highest correlation' analysis, the median rate map correlation was similar between the control and mEC lesion groups (both *p*-values ≥ 0.65, Mann-Whitney U tests) and did not deviate from chance (stippled line) for either comparison (all *p*-values ≥ 0.37, Sign and Mann-Whitney U tests). None of the rats therefore demonstrated a coordinated shift of a constant map. (**C**) Circles represent the median rate map correlation coefficient per rat and are sorted by the extent of mEC III damage. In the 'Matched cue card' and the 'Highest correlation' analysis, the amount of remapping was similar when individual rats were compared to each other (all *p* values > 0.05, Kruskal-Wallis tests). In addition, map similarity was not different from chance in each individual control and mEC-lesioned rat (all *p* values > 0.05, Sign and Mann-Whitney U tests).

SUPPLEMENTAL EXPERIMENTAL PROCEDURES

Contact for Reagent and Resource Sharing

Further information and requests for resources may be directed to and will be fulfilled by the Lead Contact, Dr. Stefan Leutgeb (sleutgeb@ucsd.edu).

Experimental Model and Subject Details

Seven experimentally naïve, male, adult Long-Evans rats, obtained from Charles River Laboratories, were used for this experiment. Of these seven rats, five received mEC lesions and two received sham lesions. Previous publications included analysis from four of the five mEC-lesioned rats (Hales et al., 2014; Schlesiger et al., 2015), and information scores and firing rates during the first 10-min session on day 1 in the novel room were previously reported for these four rats (Hales et al., 2014). However, none of the remaining data from the recordings across rooms were included in previous publications. No animals were excluded for technical reasons. All experiments were performed in the dark phase of the cycle. During the experiment, rats were food restricted and maintained at ~90% of their free-feeding body weight. Water was available ad libitum. All experimental procedures were approved by the Institutional Animal Care and Use Committee at the University of California, San Diego.

Method Details

Surgical Procedures

Medial EC lesion surgeries and sham surgeries were performed as previously described (Hales et

al., 2014). In brief, to lesion the entire dorsoventral axis of the mEC, five rats received NMDA injections at eight different DV coordinates (-5.2, -4.7, -4.2, -3.7, -3.2, -2.7, -2.2, -1.7 mm) with an infusion rate of 0.1 µl/min (0.13 µl per site). The ML coordinate was ± 4.6 mm, and the needle was angled at 22° in the posterior to anterior direction, with the needle tip immediately anterior to the transverse sinus. In control rats, a craniotomy identical to the craniotomy in mEC-lesioned rats was performed, but dura was not punctured.

For hippocampal recordings, tetrodes were constructed by twisting four 17 µm polyimide-coated platinum-iridium (90%/10%) wires (California Fine Wire, California). The electrode tips were plated with platinum at 1 kHz to reduce the impedances to 200-300 kΩ. Fourteen tetrodes were arranged into two bundles, each containing six to eight independently movable tetrodes. After the mEC or sham lesion was made, the electrode assembly was secured to the skull using stainless steel screws and dental cement. The two tetrode bundles were targeted to the hippocampus of each hemisphere (AP: 4.0 mm, ML: ±2.45 mm, angled laterally towards CA1 recording sites at approximately ML ±3.0 mm). One electrode in each hemisphere remained in the cortex and was used as a reference for differential recordings.

Recording rooms, recording chambers and random foraging behavior

Three different rooms were introduced to each rat, except for rat 714 which was introduced to an additional room during a second series of recordings. In each room, the recording system and a light source were located in proximity to the entrance, and a recording chamber was placed on a table (54-66 cm height) that was located in the center of the room. Recording chambers were

either black or white squared boxes (1 m^2) or a black cylinder (diameter, 1 m) with 50 cm high walls. A polarizing cue card (20 x 50 cm) was placed in each recording chamber at a constant position. During foraging sessions, exploratory behavior was sustained by randomly scattering cereal crumbs over the surface area of the recording chamber at intervals of ~1 min. Before, in-between and after foraging sessions, the apparatus was cleaned with water while rats rested in a transparent holding box (30 cm x 30 cm x 56 cm) that was placed on a pedestal of 106 to 116 cm height. No curtains were used to allow the rat a free view of distal cues, such as posters on the wall and shelves.

Experimental design and recordings

Rats were pretrained for 5 days in two 10-min random foraging sessions per day. One control rat and four mEC-lesioned rats were also trained on a six-arm radial maze in the same room (as described in Schlesiger et al., 2013). Rats were subjected to either sham or mEC lesion surgery after pretraining was complete. After a recovery period of 7 days, training was continued in a second room for 7 to 12 days with two to six 10-min random foraging sessions per day. The rats trained on a six-arm maze before surgery were also trained on a six-arm maze after surgery. During the period of training, tetrodes were slowly advanced into the dorsal CA1 area of the hippocampus. After placing the majority of the tetrodes in the CA1 cell layer, hippocampal recordings were performed. During tetrode advancement and during recordings, the electrode assembly was connected to a multichannel, impedance matching, unity gain preamplifier headstage. The output was routed to a data acquisition system with 64 digitally programmable differential amplifiers (Neuralynx, Tucson, AZ, USA). Spike waveforms above a threshold of

40-45 µV were time-stamped and digitized at 32 kHz for 1 ms. The rat's position was tracked at 30 Hz by recording the position of light-emitting diodes that were placed above the head. Local field potentials were acquired by recording one channel of each tetrode with the filters set to the 1-450 Hz band.

Over 3 consecutive days, recording sessions included two different rooms on each day (Figure 1). Room A was familiar to the rats (room used for pretraining before surgery: control rats 505 and 614, mEC-lesioned rats 434 and 514; room used for training after surgery: mEC-lesioned rats 587 and 645). Room B was novel to the rats at the beginning of the recording sequence. Medial EC-lesioned rat 714 was tested in two sets of two-room experiments, in the room used for pretraining before surgery and a novel room as well as in the room used for training after surgery and a second novel room. Both novel rooms are referred to as room B for data analysis. Recordings from day 1 and day 3 were analyzed for all rats except when high quality recordings could not be obtained. Only data from day 1 were therefore included for rat 587, and recordings on day 2 instead of day 3 were analyzed for rat 434. On each recording day, a total of five recording sessions were performed across the two rooms (Figure 1). The foraging sessions were separated by inter-session intervals of 5 min, and the entire block of foraging sessions was preceded and followed by rest sessions of 10–20 min.

Histology

The brains were prepared for the identification of tetrode locations in cresyl violet-stained sections. For quantification of the mEC lesion extent, we also prepared NeuN-stained sections

(1:15000, Chemicon, CloneA60) and used the Cavalieri method as previously described (Hales et al., 2014) to measure the volume of the spared tissue in mEC layer II, mEC layer III, mEC deep layers, dorsal parasubiculum, ventral parasubiculum, and hippocampus. Patches of cells that showed clear signs of disorganization (e.g., multipolar processes in pyramidal layer III cells that have otherwise apical dendrites oriented toward the cortical cell surface) and necrosis (e.g., fragmented nuclei) were counted as damaged (see Figure S1).

Data analysis

All data analysis was performed by importing position and spike data into Matlab and by further processing the data with custom-written scripts and functions.

Spike sorting, cell tracking and cluster quality. Spike sorting was performed manually using the graphical cluster-cutting software (MClust, D. Redish), which we modified in order to reliably track clusters across sessions (Mankin et al., 2012). Recordings during rest periods throughout the day were used to confirm recording stability during the experiment and to identify hippocampal cells that were silent or fired at low rates during behavior. Clustering was performed manually in two-dimensional projections of a multidimensional parameter space (consisting of waveform amplitudes, waveform energies, and the peak-to-valley difference of each of the four tetrode channels). Autocorrelation and cross-correlation functions were used as additional separation tools. Putative principal cells were distinguished from putative interneurons by spike width and average firing rate, and only putative principal cells were included in the analysis. Cluster quality was assessed by calculating the L-ratio and the Mahalanobis (i.e., isolation) distance (Schmitzer-

Torbert et al., 2005) for each cluster of spikes recorded during the random foraging task.

Rate maps. The recording enclosure was divided into 5 cm x 5 cm location bins. Spatial firing rate distributions were constructed by summing the total number of spikes that occurred in each location bin, dividing the sum by the amount of time that the animal spent in that location, and then smoothing with a 5 by 5 bin Gaussian filter with a standard deviation of approximately 1 bin (Koenig et al. 2011).

Spatial correlation. The spatial similarity between rate maps across two rooms was calculated using Pearson's correlation. We first oriented trajectory maps obtained in each of the two rooms with respect to their allocentric orientation (i.e., the east wall of the recording chamber in room A was aligned with the east wall of the recording chamber in room B) and then centered the two maps with respect to each other. For each cell, the correlation coefficient was subsequently calculated by comparing the firing rates between all overlapping spatial bins. Similarly, rate maps between two sessions in the same room were compared by calculating the correlation coefficient between spatial bins at corresponding locations. For the within-session comparisons, the first and second 10-min session in each room (see Figure 1 for experimental design; novel room: B and B' on day 1 in room B; moderately familiar room: B and B' on day 3 in room B; highly familiar room: A' and A'' on day 3 of the recording sequence) was split into two 5-min intervals, and rate maps were generated for each of those intervals. The correlation coefficient was then calculated by comparing the first and second half of each session. For both the within and across-session comparison, cells that did not reach an average firing rate of ≥ 0.25 Hz in at least one of the two

compared sessions were excluded from analysis. The chance level was determined by shuffling the cell identity for each pair of sessions before calculating correlation coefficients. The shuffling procedure was repeated 100 times, and the median correlation coefficient was taken for each comparison (range of medians: -0.01 to 0.02).

The described approach was complemented with two additional methods. (1) The trajectory maps obtained in the two rooms were oriented with respect to the polarizing cue card (which was offset by either 90 or 270 degrees between the rooms) and the Pearson's correlation was subsequently calculated as described above. (2) For each cell, one of the maps was analytically rotated in steps of 90 degrees, the Pearson's correlation was calculated for each of the four possible comparisons, and the highest correlation coefficient from these comparisons was selected for further analysis.

Firing field boundaries. Place fields were defined by identifying areas of at least 8 adjacent pixels with a peak firing rate of at least 2 Hz. Starting from the peak, the field boundaries were found by building contours outwards until a threshold of 20% of the field's peak firing rate was reached. If any remaining peaks with a firing rate ≥ 2 Hz remained outside of an already defined field, the procedure was repeated. The field with the highest peak rate was retained as the cell's place field.

Distances between place fields. The distances between place field peaks were calculated for each pair of simultaneously recorded cells when each cell in the pair had at least one field over two consecutive recording sessions, either within the same room or across two different rooms

(within-room comparisons: day 3, A' and A''; across-room comparisons: day 3, A' and B'; see Figure 4A for schematic). Pearson's correlations were used to compare the place field distances between either two sessions in the same room (A' and A") or two sessions in different rooms (A' and B').

Spatial information. The information score was calculated for cells with average firing rates of ≥ 0.25 Hz. It describes the information density per spike and was calculated as described by Skaggs and colleagues (1993):

$$I = \sum_i p_i \frac{\lambda_i}{\lambda} \log_2 \frac{\lambda_i}{\lambda}$$

where I is the information density measured in bits per spike, i is the index of the pixels of the place field, P_i is the probability of the rat being at location i, λ_i is the average firing rate of the cell when the rat is at location i and λ is the total average firing rate.

Statistical analysis. All statistical tests were two-sided with $\alpha = 0.05$. To compare the proportion of active cells between groups, Chi-square tests were used. For all remaining statistical analysis, Kolmogorov-Smirnov tests were first performed to test for normality. Because all tested distributions were non-normal, equality of medians was tested with Mann-Whitney *U* tests and Kruskal-Wallis tests for between-group comparisons, and Wilcoxon signed-rank tests and Friedman tests for within-group comparisons. Sign tests were used to test the samples against chance. Multiple comparisons were corrected with the Holm-Bonferroni procedure, and Tukey-Kramer tests were used for post hoc analysis.

Resources Table

REAGENT or RESOURCE	SOURCE	IDENTIFIER
Antibodies		
Mouse monoclonal NeuN antibody	Chemicon	Clone A60
Biotinylated anti-mouse IgG	Vector BA-2000	
Biological Samples		
Chemicals, Peptides, and Recombinant Proteins		
Isoflurane	MWI	Cat #: NDC 13985-528-60
Buprenorphine	MWI	Cat #: 29308
Plantinic acid for platinum plating	Sigma-Aldrich	Cat #: 206083; CAS 18497-13-7
Sodium pentobarbital	MWI	Cat #: 15199
Formaldehyde	EMD	Cat #: FX-0415-4; CAS 50-00-0
Cresyl violet	EMD	Cat #: M-19012; CAS 10510-54-0
N-methyl-D-aspartate	Tocris	Cat #: 0114
Experimental Models: Organisms/Strains		
Long Evans rats	Charles River Labs	RRID: RGD_2308852
Software and Algorithms		
MClust	A.D. Redish	http://redishlab.neuroscience.umn.edu/MClust/MClust.html
Matlab v 2015b	Mathworks	RRID: SCR_001622
StereoInvestigator	MBF Bioscience	
Other		
Hyperdrive	Custom built; designed by B.L. McNaughton	US Patent: US5928143 A
Platinum-Iridium tetrode wire	California Fine Wire Company	Cat #: CFW0011873
Freezing microtome	Leica	Model: SM 2000R
Digital Neuralynx recording system	Neuralynx	Model: Digital Lynx SX

SUPPLEMENTAL REFERENCES

Koenig J., Linder A. N., Leutgeb J. K. & Leutgeb S. (2011). The spatial periodicity of grid cells is not sustained during reduced theta oscillations. *Science*, 332(6029):592-5.

Hales, J. B., Schlesiger, M. I., Leutgeb, J. K., Squire, L. R., Leutgeb, S. & Clark, R. E. (2014). Medial entorhinal cortex lesions only partially disrupt hippocampal place cells and hippocampus-dependent place memory. *Cell Rep,* 9**,** 893-901.

Mankin, E. A., Sparks, F. T., Slayyeh, B., Sutherland, R. J., Leutgeb, S. & Leutgeb, J. K. (2012). Neuronal code for extended time in the hippocampus. *Proc Natl Acad Sci U S A,* 109**,** 19462-7.

Skaggs, W. E., McNaughton, B. L., Gothard, K. M. & Markus, E. J. (1993). An information-theoretic approach to deciphering the hippocampal code. *Advances in Neural Information Processing Systems 5* (eds. Hanson, S. J., Giles, C. L. & Cowan, J. D.) 1030-1037 (Morgan Kaufmann, San Mateo).

Schlesiger, M. I., Cannova, C. C., Boublil, B. L., Hales, J. B., Mankin, E. A., Brandon, M. P., Leutgeb, J. K., Leibold, C. & Leutgeb, S. (2015). The medial entorhinal cortex is necessary for temporal organization of hippocampal neuronal activity. *Nat Neurosci*, 18, 1123-32.

Schlesiger, M. I., Cressey, J. C., Boublil, B., Koenig, J., Melvin, N. R., Leutgeb, J. K. & Leutgeb, S. (2013). Hippocampal activation during the recall of remote spatial memories in radial maze tasks. *Neurobiol Learn Mem,* 106**,** 324-33.

Schmitzer-Torbert N., Jackson J., Henze D., Harris K. & Redish A. D. (2005). Quantitative measures of cluster quality for use in extracellular recordings. *Neuroscience*, 131(1): 1-11.